# Low-cost interrogation of long-distance and multi-point FBG sensor using incoherent-FMCW optical ranging system



| メタデータ | 言語: eng |
| --- | --- |
| | 出版者: |
| | 公開日: 2020-08-07 |
| | キーワード (Ja): |
| | キーワード (En): |
| | 作成者: |
| | メールアドレス: |
| | 所属: |
| URL | https://doi.org/10.24517/00059006 |

# Low-Cost Interrogation of Long-Distance and Multipoint FBG Sensor using Incoherent-FMCW Optical Ranging System

Dwi Hanto, *Member, IEEE,* and Koichi Iiyama, *Member, IEEE*

***Abstract*—More than a decade, multipoint sensor systems involving fiber Bragg gratings (FBGs) have been widely used in various implementations, especially the structural health monitoring system (SHMS). In this paper, a three-points FBG sensor was successfully analyzed by combination of incoherent frequency modulated continuous wave (I-FMCW) optical ranging system and a vertical-cavity surface-emitting laser (VCSEL) as a wavelength-tunable laser source. This system is not only capable of reading out the FBG sensors, but also identifying the location of the installed FBGs. The I-FMCW can be conducted by intensity modulation of a low-cost commercial VCSEL. Furthermore, the wavelength of the VCSEL can also be tuned by the injection current change to match the Bragg wavelength of FBGs. The detected signal from the FBGs and the reference signal from the signal generator are electrically mixed to obtain the beat frequency. A thermo-electric controller (TEC) controls temperature of one of the FBGs in the range of 25ºC ~ 45ºC, and contrary the others are kept at room temperature. As well as measuring temperature, one of the FBGs is strained in the range of 369 με ~ 2137 με. The measurement result shows that the system can clearly distinguish all FBGs installed in totally 6.6 km-long optical fiber. In addition, the Bragg wavelength shift of the FBGs according to temperature as well as strain changes was successfully measured. The system can be scaled up more than three FBGs and extended scale area, and is a candidate as a low-cost and simple FBG interrogator for a long-range SHMS.**

***Index Terms*— FBG, VCSEL, incoherent-FMCW, SHMS**

## I. Introduction

Nowadays, engineers, researchers, and stakeholders are still struggling with how to manage massive structures, including long-term maintenance and damage prevention. Fortunately, many advances in sensing, computing, and communication technologies create a new technical field to monitor the structures, such as the structural health monitoring systems (SHMS). This system is a process of implementing a damage detection and characterization strategy for engineering structures. The advantage of using the SHMS is that the structures can be monitored in real-time to predict damage of the structure [1].

The SHMS aims to detect, identify, locate, and assess defects that may affect safety or performance of structures. The SHMS usually employs many kinds of sensors such as a strain gauge, a piezoelectric sensor, a microelectromechanical (MEMS) sensor, an eddy current sensor, and a fiber optic sensor. A fiber-optic sensor is very compact and can be easily embedded into structures, and hence is suitable for structural monitoring [2]. A fiber-optic sensor widely used in the SHMS is a fiber Bragg grating (FBG) because various physical quantities such as strain and temperature at several locations can be measured [3].

FBG is a fiber optic device that has a periodic refractive index variation in the core. When broad-spectrum light is incident to the FBG with negligible attenuation, only the light whose wavelength satisfies the Bragg condition is strongly reflected. The Bragg condition can be expressed as;

$$\lambda_B = 2n\Lambda \tag{1}$$

where $\lambda_B$ is the Bragg wavelength, $n$ is the effective refractive index, and $\Lambda$ is the period of the refractive index change of the FBG. Due to temperature ($T$) and strain ($\varepsilon$) dependence of the parameters $n$ and $\Lambda$, the $\lambda_B$ is accordingly changed. The Bragg wavelength shift due to strain and temperature changes can be described as [4];

$$\Delta\lambda_B = \lambda_B[(1 - P_e)\varepsilon + (\alpha_\Lambda + \xi_n)\Delta T] \tag{2}$$

where $P_e$ is the effective strain-optic constant, $\alpha_\Lambda$ is the thermal expansion coefficient, and $\xi_n$ is the thermo-optic coefficient of the fiber.

The Bragg wavelength shift is usually measured using an optical spectrum analyzer (OSA). Because of the limited scanning speed and high-cost of an OSA, a charge-coupled device (CCD) spectrometers is successfully used instead of an OSA [5]. However, it may be rather difficult to apply it for long-range FBG sensing because high power broad-spectrum light source is needed. Moreover, some researchers have proposed alternative methods which are compact, low-cost, and effective in real-time applications. These methods are generally

The first author gratefully thanks to Program for Research and Innovation in Science and Technology (RISET-Pro) Scholarship, World Bank Loan No. 8245-ID, provided by the Ministry for Research, Technology and Higher Education, Republic of Indonesia.

Dwi Hanto is with the Division of Electrical Engineering and Computer Science, Kanazawa University and also with Research Center for Physics, Indonesian Institute of Sciences (LIPI) (email:dwi.hanto@lipi.go.id).

Koichi Iiyama is with the Division of Electrical Engineering and Computer Science, Kanazawa University (email: iiyama@se.kanazawa-u.ac.jp).

.

classified into three categories; (a) utilizing interferometric demodulation, (b) using a tunable filter, and (c) using a tunable laser. The third method is now widely employed for FBG sensor interrogation due to its high intensity, narrow lasing spectrum and wide wavelength tuning range [6]. Occasionally, it is also called the wavelength-swept laser method.

Now, many kinds of wavelength-swept lasers have been proposed and commercialized as external cavity tunable lasers using a fiber Fabry-Perot (FFP) filter, a polygonal mirror scanner, and Fourier-domain mode-locking (FDML) [7]. However, those techniques might require a high-cost specific element for wavelength selection and sweep. A vertical-cavity surface-emitting laser (VCSEL) is a low-cost wideband wavelength-tunable laser source. By simply changing the injection current without additional optical and mechanical elements, Moon et al. reported that a VCSEL could be wavelength-swept up to 10 nm for the sweep rate up to 100 kHz [8]. Since the Bragg wavelength shift of a FBG is usually less than 10 nm [9], a wavelength-swept laser source using a VCSEL is suitable to interrogate the FBGs.

For health monitoring of huge structures, multipoint FBG sensors may be used. Stakeholders need to know the quantity and location where the damage will be occurred for further evaluation. Many FBGs with different Bragg wavelengths are usually installed for multipoint sensing, and the locations of the FBG sensors are found from the Bragg wavelength of the FBG. In this case, allowable Bragg wavelength shift is limited to less than the minimum Bragg wavelength separation between FBGs to avoid crosstalk between FBG sensors. Large Bragg wavelength separation limits the number of sensors because of limited spectral bandwidth of a laser source. Several FBGs can be multiplexed with wavelength division multiplexing (WDM) and time-division multiplexing (TDM). However, the number of sensors are also limited by the spectral bandwidth of the light source, the spectral bandwdith of the sensor window, and the spatial resolution of individual sensor [10].

The other methods for identifying multipoint FBGs is to combine the multipoint FBGs with optical reflectometry such as (a) optical time-domain reflectometry (OTDR), (b) two-photon absorption (TPA), and (c) optical frequency domain reflectometry (OFDR). The location and the Bragg wavelength shift of each FBG can be identified from the reflection profile of optical reflectometry for each wavelength. Therefore, there is no restriction on the Bragg wavelength shift and the number of sensors. Since the OTDR uses optical pulses, the OTDR has problems with a dead zone and tradeoff between the spatial resolution and the signal noise to ratio (SNR) due to narrowing the pulse width [11]. The TPA, which uses two laser diodes with different wavelength, has an excellent spatial resolution but the photocurrent may be unstable [12].

The OFDR is classified into two categories; a coherent OFDR (C-OFDR) and an incoherent OFDR (I-OFDR). The C-OFDR utilizes interference of lightwave from a target and a reference lightwave. Hariyama et al. reported the accurate C-OFDR using a VCSEL with the accuracy of 10 μm for limited measurement range of 2 m [13]. The C-OFDR requires a narrow linewidth laser and ultra-linearly swept optical source when it will be applied in long-range measurement. On the other hand, since the I-OFDR is non-interferometric method, it has a possibility for long-range measurement [14] more than the C-OFDR. Therefore, it may be appropriate to be applied in long-range structures like bridges or dams.

One type of the I-OFDR is to measure the frequency response of the target by using a vector network analyzer, and the location of the target is calculated by inverse Fourier transform of the frequency response. By using this system, 20 FBGs can be successfully interrogated using a tunable laser source and an external light modulator [15].

The other type of the I-OFDR is an incoherent frequency modulated continuous wave (I-FMCW) optical ranging system. Fig. 1 shows the configuration of the I-FMCW optical ranging system. The I-FMCW optical ranging system is composed of an intensity-modulated laser source whose modulation frequency is linearly swept in time. The beat signal between the reflected light from the target and the modulation signal (reference signal) is obtained by using the double-balanced mixer (DBM) and the low pass filter (LPF). Fig. 2 shows the instantaneous modulation frequency of the reflected and the reference signals. The reflected signal is delayed by $\tau$ with respect to the reference signal due to the distance to the target, and the mixed signal of the two signals has a beat frequency corresponding to the distance to the target.

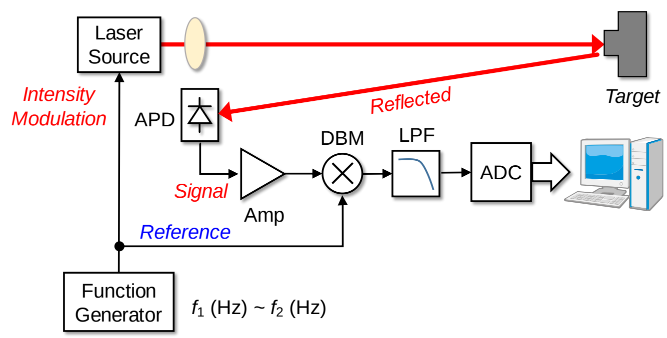


Fig. 1. Configuration of I-FMCW optical ranging system.

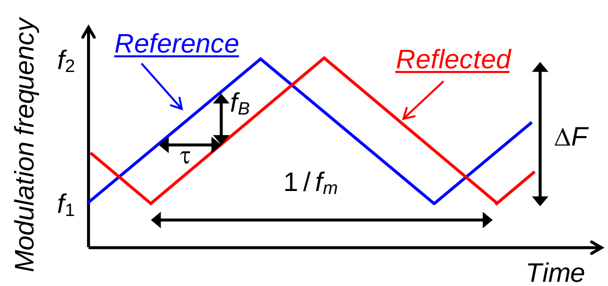


Fig. 2. Modulation frequency of the reference and the reflected signals of I-FMCW optical ranging system.

In this paper, we propose an I-FMCW optical ranging system using a VCSEL for interrogating multipoint FBG sensors. To explore the spectrum of FBGs, we use a VCSEL as a wavelength-tunable laser source because of its wide wavelength tuning range with smaller injection current change. Compared with other techniques, it needs only a low-cost component. For long-range remote SHMS, a thousand number of FBG is needed to obtain complete information. Due to cost and energy constraints, only a small number of FBG is used to describe the entire structures [11] for instance 17 FBGs for 300 m bridge in reference [16]. In our experiment, we demonstrate three-points FBG sensors installed in a totally 6.6 km-long optical fiber for the purpose of long-range SHMS. We also discuss the spatial resolution, performance of the FBG as temperature and strain sensors, and long-term temperature monitoring. According to the best of our knowledge, this system offers a less-expensive solution than another FBG interrogator currently available.

## II. Experiments

The experimental setup of the FBG interrogator using the I-FMCW optical ranging system is illustrated in Fig. 3. A single-mode VCSEL emitting at 1560 nm is used as a laser source. The temperature of the VCSEL is controlled to 20ºC. The VCSEL is sinusoidally intensity-modulated by the injection current modulation, and the modulation frequency is linearly swept in time from 10 MHz to 160 MHz with 50 Hz repetition frequency by the signal generator (SG: DG4162 form RIGOL). The emitted light from the VCSEL was amplified up to 6 dBm by using the erbium-doped optical fiber amplifier (EDFA) and is then launched into single-mode fibers containing three FBGs (FBG1, FBG2, and FBG3) through the circulator. The specification of FBG1, FBG2, and FBG3 are shown in Table I.

TABLE I
SPECIFICATION OF FBG1, FBG2, AND FBG3.

| | Bragg wavelength (nm) | Reflectivity (%) | Bandwidth (nm) |
|---|---|---|---|
| FBG1 | 1560.01 | 5.59 | 0.083 |
| FBG2 | 1560.04 | 5.81 | 0.110 |
| FBG3 | 1560.03 | 6.24 | 0.095 |

The reflected light from the FBGs are detected with the photodetector (PD). The wavelength of the VCSEL is controlled by the injection current to measure the reflection spectrum of the FBGs. To confirm the possibility of remote sensing, we insert optical fibers, FO1, FO2, and FO3 between FBGs. The lengths of FO1 and FO2 are 1000 m and 5640 m, respectively, and the length of FO3 is selected from 40 m, 10 m, and 5 m. The ranging signal is generated by electrical mixing of the reflected signal and the reference signal by using the double-balanced mixer (DBM) followed by the low pass filter (LPF), and then the ranging signal is sampled using the high-speed data acquisition (DAQ) board (MC USB-2020 from Measurement Computing). The data acquisition board has two analog input channels with the sampling rate until 20 MS/s and 12-bit resolution.

The modulation bandwidth of the VCSEL including the VCSEL mount is 500 MHz, and the 3 dB bandwidth of the PD (including the following amplifier) is 150 MHz. The group delay from the VCSEL to the PD is constant up to 500 MHz. Although the 3 dB bandwidth of the PD is slightly narrower than the maximum modulation frequency, no compensation of the frequency response was needed and applied.

The working principle of the FBG Interrogator is described as following. The reflected signal detected by the PD *s*(*t*), the reference signal *r*(*t*), and the electrically mixed signal by the DBM *m*(*t*) are expressed as;

$$\begin{aligned} r(t) &= A\cos(2\pi f t) \\ s(t) &= B\cos\{2\pi(f-\gamma\tau)t\} \\ m(t) &= r(t)\times s(t) \\ &= \frac{AB}{2}\left[\cos\{2\pi(2f-\gamma\tau)t\} + \cos(2\pi\gamma\tau t)\right] \\ f_b &= \gamma\tau = 4nf_m\Delta F.\frac{L}{c} \end{aligned} \tag{3}$$

where $A$ and $B$ are the magnitudes of the reference and the reflected signals, respectively, $f$ is the instantaneous modulation frequency of the reference signal at a certain time, $\gamma$ is the modulation frequency sweep rate in Hz/s unit, $t$ is the time, $\tau$ is the delay time between the reflected and the reference signals, $f_b$ is the beat frequency, $f_m$ is the repetition frequency of the modulation frequency sweep, $\Delta F$ is the sweep range of the modulation frequency, $L$ is the location of the FBG, $n$ is the refractive index of optical fibers, and $c$ is the speed of light in vacuum. The modulation frequency sweep rate $\gamma$ is given as $\gamma = 2 f_m \Delta F$ from Fig. 2, and the delay time $\tau$ is given as $\tau = 2nL/c$ considering the roundtrip propagation. As shown in the above equation, the mixed-signal $m(t)$ has the beat frequency $f_b$ corresponding to the distance to the reflection point [17]. Since three FBGs are used in our study, three different beat frequencies are observed.

The I-FMCW optical ranging system is controlled with a program using LabVIEW (from National Instruments). In order to sweep the wavelength of the VCSEL, the injection current of the VCSEL is changed in stepwise [8] by using the programmable voltage source. The wavelength change due to the injection current change of the VCSEL is measured by using an OSA, and the result is shown in Fig. 4. The obtained relationship between the injection current and the wavelength is $\lambda$ (nm) = 0.5696 ILD (mA) + 1557.3, where ILD is the injection current of the VCSEL, and the relation is stored in the program and is used to define the wavelength of the VCSEL from the measured injection current (ILD signal) which is acquired by the analog input channel 1 of the DAQ board.

The modulation frequency sweep is bidirectional with 10 ms of the frequency increasing section and 10 ms of the frequency decreasing section, and the ranging signal in the frequency increasing section is acquired with the analog input channel 0 of the data acquisition (DAQ) board. The fast Fourier transform (FFT) is carried out to obtain the beat spectrum in order to determine the position of the FBGs by using eq.(3). By applying a peak searching, the system can also recognize where and which FBG is being read. Lastly, the program also provides some features such as plotting and storing data.

The analyzed data from each FBG is depicted as a spectrum region as shown in Fig. 5. The Bragg wavelength $\lambda_B$ can be estimated by using the centroid peak-tracking method shown in the following equation [18]:

$$\lambda_B = \frac{\sum_{i=1}^{N}\lambda_i . M_i}{\sum_{i=1}^{N} M_i} \tag{4}$$

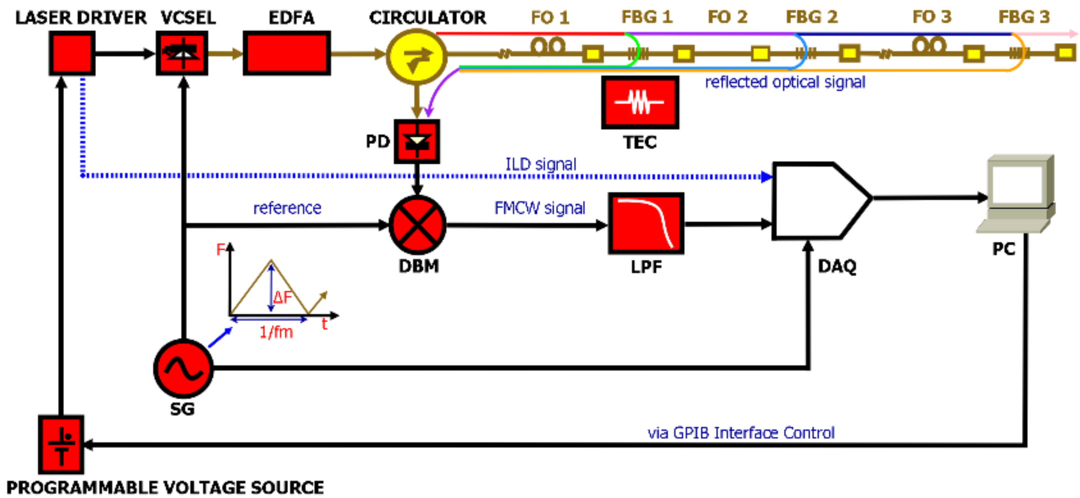


Fig. 3. Block diagram of FBG Interrogator based on I-FMCW optical ranging system.

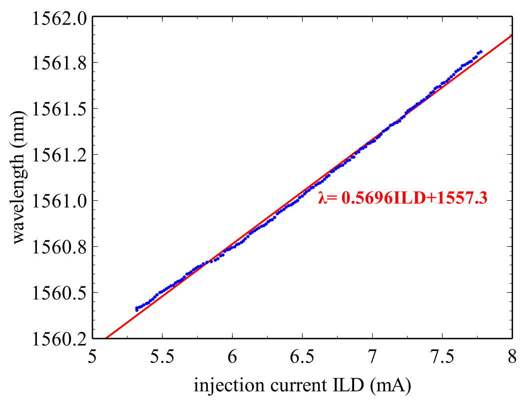


Fig. 4. Wavelength shift of a VCSEL by the injection current change.

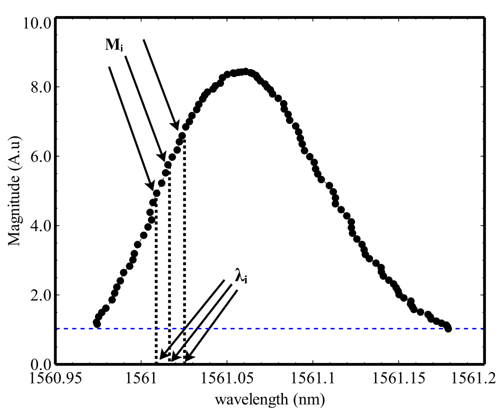


Fig. 5. Sketch of the centroid peak-tracking method [18].

where $\lambda_i$ is the wavelength of the VCSEL at the $i$-th point, $M_i$ is magnitude of the beat frequency at the $i$-th point, and $N$ is the number of data whose magnitude $M_i$ is higher than a given threshold shown as a dashed line in Fig. 5. The estimated Bragg wavelength $\lambda_B$ is used to measure the physical quantity (temperature and strain in this experiment).

For temperature measurements, ambient temperature of FBG1 is changed in the range of 25ºC ~ 45ºC by using a thermoelectric controller (TEC) in order to validate the FBG interrogator. Contrary, FBG2 and FBG3 are kept in room temperature. For strain measurements, we applied strain to FBG3 using the cantilever beam method [19]. FBG3 is glued on the top surface of aluminum plate with 400 mm-long, 20 mm-wide, and 3 mm-thick. Many kinds of load are applied at the free end of the cantilever beam so that the FBG3 is strained from 369 με ~ 2137 με. We then demonstrate and analyze the performance of the system including long-distance and multipoint capabilities, the spatial resolution, the spectrum response, and long-term stability.

## III. Long-Range and Spatial Resolution

In the SHMS, precise location identification for long measurement range is required because the monitored structure is huge. To confirm long-range measurement, we measured the Fresnel reflections at the output facets of a 1000 m-long and a 6640 m-long optical fibers without FBGs. The result is shown in Fig. 6. The Fresnel reflection peak for the 6640 m-long optical fiber is clearly found, however, the magnitude is weaker than the Fresnel reflection peak for the 1000 m-long optical fiber due to the attenuation of the fiber. Nevertheless, the SNR for the 6640 m-long optical fiber is 27 dB, indicating that our system might be a possibility for long-range SHMS.

We then installed FBGs into a long-range I-FMCW optical ranging system over 6.6 km in length. The lengths of FO1 and FO2 in Fig. 3 are 1000 m and 5640 m, respectively, in order to validate the capability of long-range FBG sensing, and the length of FO3 in Fig. 3 is short (40 m, 5 m, or 3 m) to confirm the spatial resolution and identify the exact location of FBG. The measured beat spectrum is shown in Fig. 7. The length of FO3 is 40 m for Fig. 7(a), 5 m for Fig. 7(b), and 3 m for Fig. 7(c). Three reflection peaks from three FBGs at same temperature are clearly observed in all Fig. 7. Two FBG spectra separated by 3 m are clearly measured as shown in Fig. 7(c) because the full-width at half maximum (FWHM) is 1.5 m in our system. This result suggests that the distance between two FBGs on the SHMS based on I-FMCW should be more than 1.5 m. Nevertheless, the distance between FBG about 1 m is sufficient for monitoring most civil structures [20].

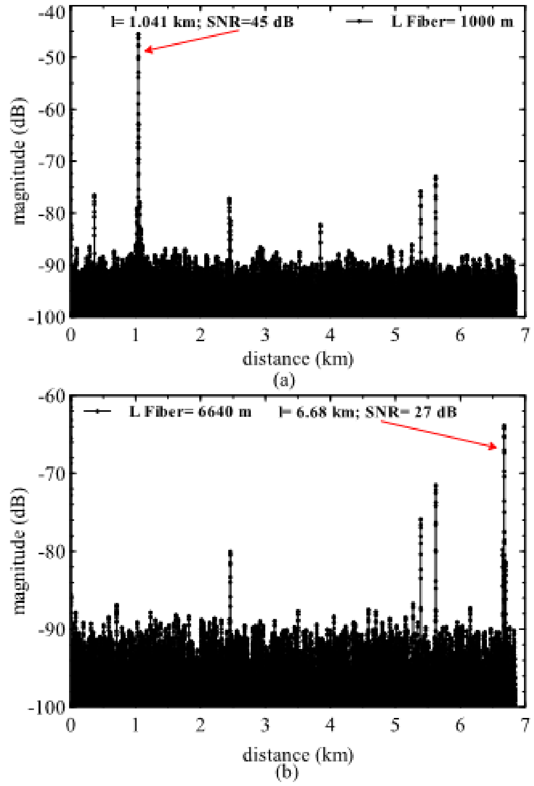


Fig. 6. Measured beat spectrum of Fresnel reflection from far end of an optical fiber with length of (a) 1000 m and (b) 6640 m.

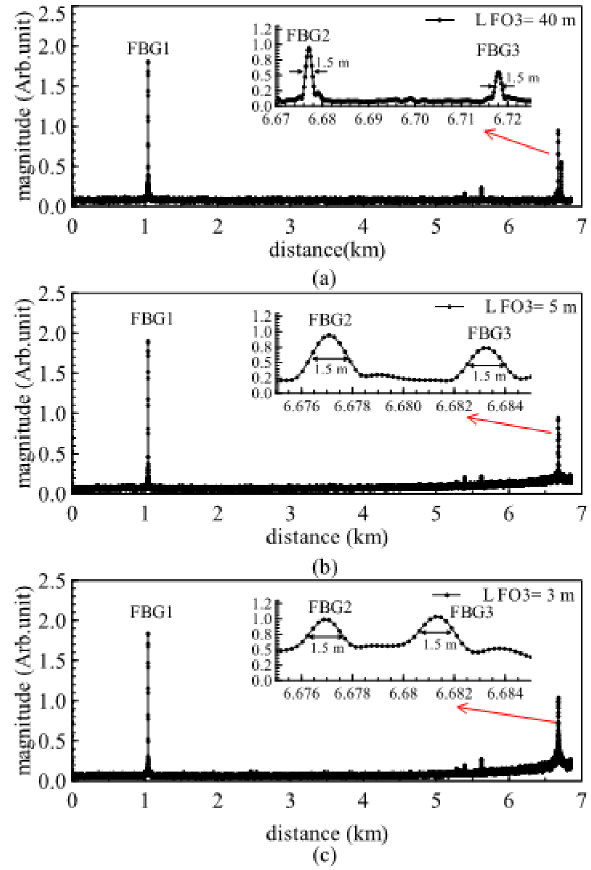


Fig. 7. Measured beat spectrum for different FO3 length, (a) 40 m, (b) 5 m, (c) 3 m at the same temperature.

Now, we discuss the spatial resolution of the I-FMCW spectrum. The spatial resolution is determined by the sweep range of the modulation frequency. The spatial resolution $\Delta l_{\mathrm{FMCW}}$ is given by the Rayleigh resolution as;

$$\Delta l_{\mathrm{FMCW}} = \frac{c}{2n\Delta F} \tag{5}$$

where $\Delta F$ is the sweep range of the modulation frequency, $n$ is the refractive index, and $c$ is the speed of light in vacuum. In our study, $\Delta F$ = 150 MHz, and then $\Delta l_{\mathrm{FMCW}}$= 69 cm for $n$ = 1.45. A Hanning window is used in the FFT, and then the beat spectrum is broadened. The spatial resolution was evaluated from the FWHM of the beat spectrum. The FWHM of the beat spectrum after multiplying a Hanning window to the I-FMCW ranging signal, $\Delta l_{\mathrm{FWHM}}$, is given as [21];

$$\Delta l_{\mathrm{FWHM}} = 2 \times \Delta l_{\mathrm{FMCW}} = \frac{c}{n\Delta F} \tag{6}$$

and $\Delta l_{\mathrm{FWHM}}$ = 1.38 m in this study. The experimental FWHM shown in Fig. 7 is the same with the theoretical FWHM. The FWHM can be easily enhanced by increasing the sweep range of the modulation frequency $\Delta F$ by using a wideband sweep generator.

Fig. 7 also shows the ability of our system to identify the precise location of the FBGs sensor. The measured locations of FBGs is tabulated in Table II. The measured locations of the FBGs are almost the same with the installed position by comparing it to the length of FO1, FO2, and FO3.

TABLE II
FBGs LOCATION IDENTIFICATION.

| Figure | Location of FBG1 (km) | Location of FBG2 (km) | Location of FBG3 (km) |
|---|---|---|---|
| 7(a) | 1.0410 | 6.6771 | 6.7181 |
| 7(b) | 1.0410 | 6.6771 | 6.6831 |
| 7(c) | 1.0410 | 6.6771 | 6.6813 |

## IV. TEMPERATURE MEASUREMENT

Using the length of optical fibers as Fig. 7(a), ambient temperature of FBG1 is set at 40ºC, but FBG2 and FBG3 are still kept at room temperature. The injection current of the VCSEL is changed from 5.21 mA to 6.85 mA with 3.28 μA step, which corresponds to the wavelength change from 1560.27 nm to 1561.20 nm with 1.87 pm step. The I-FMCW optical ranging was carried out 50 ms after the injection current change so that the wavelength of the VCSEL is stable. Totally the I-FMCW optical ranging was carried out 500 times for the above wavelength range, and the total measurement time is 90 sec.

The measured results are shown in Fig. 8(a) and (b), where the wavelength of the VCSEL is tuned to 1560.740 nm and 1560.955 nm, respectively. In Fig. 8 (a), two peaks for FBG2 and FBG3 are shown because the tuned wavelength corresponds to the Bragg wavelength of the FBG around room temperature. On the other hand, only one peak corresponding to the FBG1 is appeared in Fig. 8(b) because the tuned wavelength corresponds to the Bragg wavelength at approximately 40ºC.

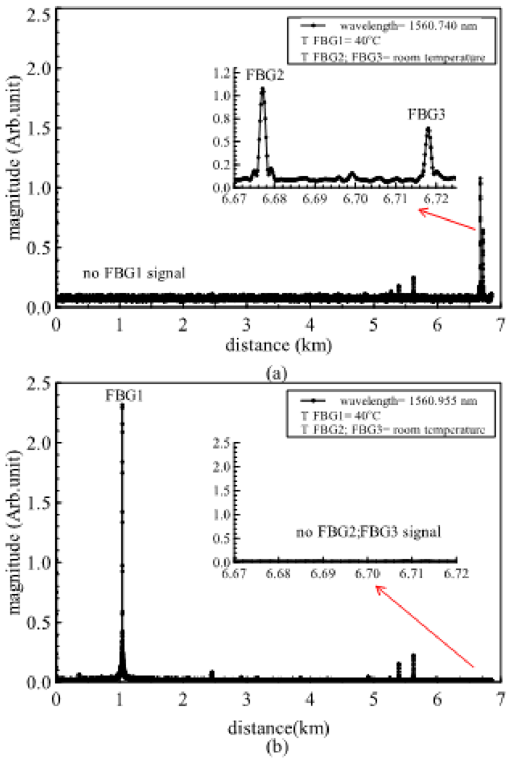


Fig. 8. Measured beat spectrum for wavelength of (a) 1560.740 nm and (b) 1560.955 nm. The temperature of the FBG1 is 40ºC, and the temperature of the FBG2 and FBG3 are room temperature (approximately 23ºC).

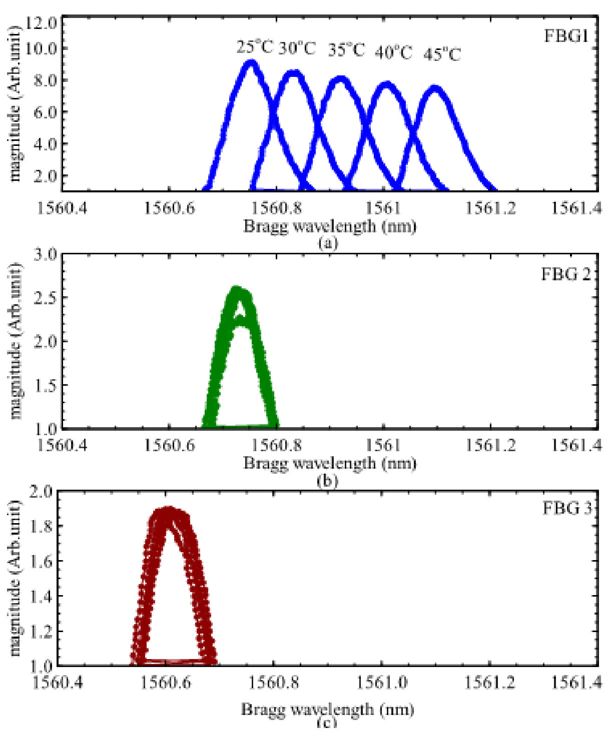


Fig. 9. Spectrum of (a) FBG1, (b) FBG2, and (c) FBG3 when the temperature of FBG1 is changed.

We measured the Bragg wavelength shift of the FBGs against the temperature change to evaluate the temperature sensitivity. The ambient temperature of FBG1 is increased from 25ºC to 45ºC in 5ºC step, and the temperature of FBG2 and FGB3 was kept at room temperature. Fig. 9 shows the shift of the FBG reflection spectra of (a) FBG1, (b) FBG2, and (c) FBG3. The reflection spectrum of FBG1 is shifted to longer wavelength according to the temperature increase, while the reflection spectra of FBG2 and FBG3 are almost unchanged because the room temperature is almost constant.

Fig. 10 shows the correlation between the temperature and the Bragg wavelength of FBG1. The Bragg wavelength is linearly increased with the temperature as expressed in eq. (2) and the reports by Song et al. [22]. From the expression shown in Fig. 10, the temperature sensitivity of FBG1 is 17.3 pm/ºC and is almost the same as a typical FBG, which is 11.6 pm/ºC. The Bragg wavelength shift against the temperature change is compared to the result measured by an OSA and an amplified spontaneous emission (ASE) as a broadband light source. The result is also shown in Fig. 10. Both results show almost the same trends and correlations.

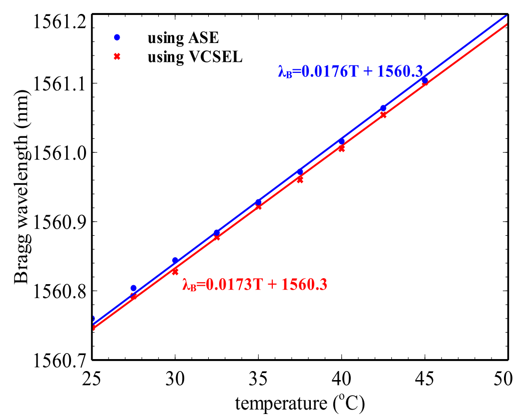


Fig. 10. Correlation between the temperature and the Bragg wavelength as a temperature sensor.

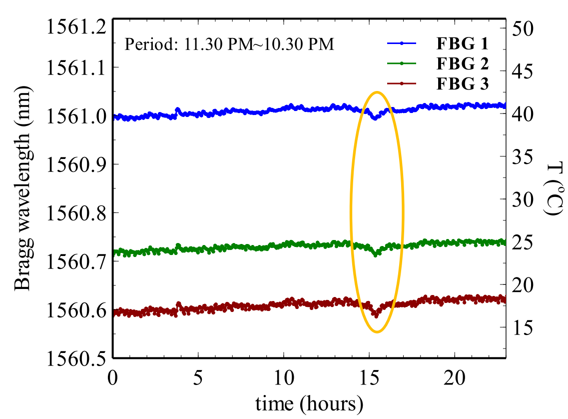


Fig. 11. Stability and reliability testing.

A critical factor in practical SHMS is long-term stability. Fig. 11 shows the Bragg wavelength of FBG1, FBG2, and FBG3 for 23 hours in our laboratory. During the experiment, FBG1 was kept at 40ºC, and FBG2 and FBG3 were kept at room temperature. The Bragg wavelength of FBG1 is almost stable at 1561 nm which corresponds to 40ºC, and the Bragg wavelengths of FBG2 and FBG3 are 1560.7 nm and 1560.6 nm, which correspond to 24ºC, and 18ºC, respectively. Around 15 hours from the initial test (with a circle marked in Fig. 11), the Bragg wavelengths of all the FBGs are slightly decreased for short time because our laboratory was opened for several minutes and then the temperature of FBG1, FBG2 and FBG3 was slightly changed at this time. The root-mean-square error (RMSE) for the FBG1 is as low as 0.6ºC. This result shows that the system is well stable for long-term operation. The RMSE of FBG2 and FBG3 are 0.6ºC, and 0.7ºC, respectively, irrespective of uncontrolled room temperature. This means the room temperature is also constant for 23 hours.

## V. STRAIN MEASUREMENT

Next, we applied our system to strain measurement. FBG1 and FBG2 are unstrained, whereas FBG3 is strained at 722 με. The measured result is shown in Fig. 12. Two peaks corresponding to FBG1 and FBG2 are measured when the wavelength is tuned to 1560.703 nm as shown in Fig. 12(a), which corresponds to the Bragg wavelength of unstrained FBG. Conversely, when the wavelength is tuned to 1561.187 nm, only the peak of FGB3 is measured as shown in Fig. 12(b), which corresponds to the Bragg wavelength of FBG strained approximately 722 με.

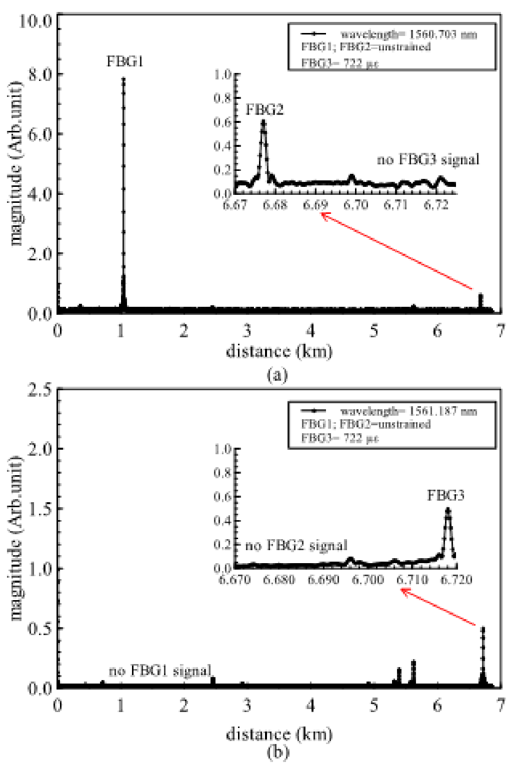


Fig. 12. Measured beat spectrum for wavelength of (a) 1560.703 nm, (b) 1560.187 nm. FBG1 and FBG2 are unstrained, and FBG3 is strained at 722με.

The Bragg wavelength shift of the FBGs as a function of the strain change is measured. FBG1 and FBG2 are unstrained and FBG3 is strained in the range of 369 με ~ 1076 με. The measured beat spectra are shown in Fig. 13(a), (b) and (c) for FBG1, FBG2 and FBG3, respectively. The Bragg wavelength of FBG3 is shifted to longer wavelength with the strain, however the Bragg wavelength of FBG1 and FBG2 are almost unchanged because FBG1 and FBG2 are unstrained.

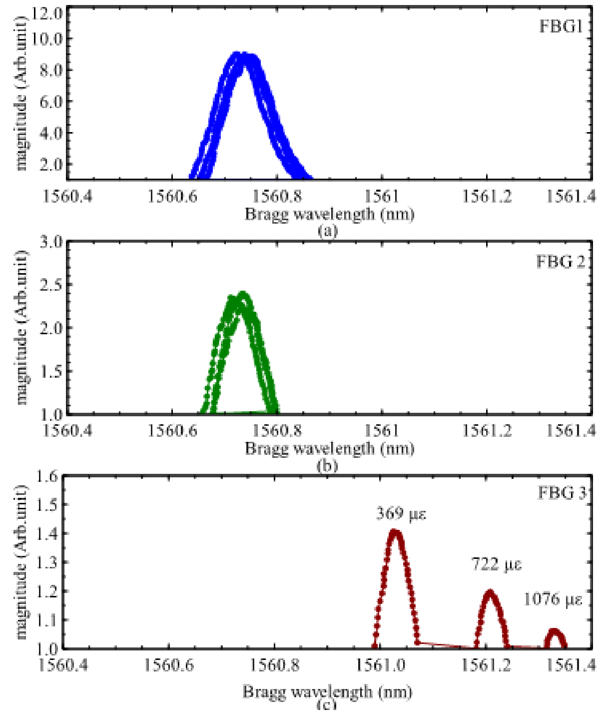


Fig. 13. Spectrum of (a) FBG1, (b) FBG2, and (c) FBG3 when FBG3 is strained and FBG1 and FBG2 are unstrained.

Fig. 14 shows the correlation between the strain and the Bragg wavelength of the FBG. The Bragg wavelength is also linearly changed with the strain, and the strain sensitivity is 0.29 pm/με, which is lower than a typical FBG strain sensitivity of 1.2 pm/με [2]. The relatively low sensitivity may be due to not optimized fixing of the FBG to the cantilever beam. The Bragg wavelength shift against the strain change is also compared to the measurement result measured by an OSA and an ASE as a broadband light source. The result is also shown in Fig. 14. Both results show almost the same trends and correlations.

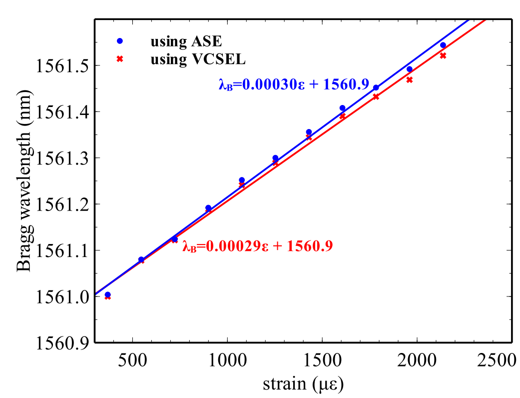


Fig. 14. Transfer function of FBG as a strain sensor.

Since FBGs are sensitive to both strain and temperature, cross-sensitivity between them is a problem. Several methods have been reported to overcome the problem, such as a combination of FBG and Fabry Perot interferometer, superstructure method [2], FBG reference [23], and coating with a polymer material [24], and these methods are easily applied to our system.

In the proposed system, the magnitude from the FBGs installed at distant location is decreased because the Bragg wavelength of all the FBGs are almost same, and then the number of FBGs may be limited. However, this problem can be solved by optimization of the optical power of the laser source and the reflectivity and the bandwidth of FBGs.

## VI. Conclusion

We have developed an FBG interrogator using the I-FMCW optical ranging system using a VCSEL, and tested for temperature and strain sensor. Since our system uses commercially available VCSEL as a wavelength-tunable laser source, our system offers low-cost FBG interrogator as comparing with other techniques. The developed system has great potential for remote SHMS because the system is able to identify the location of sensors from the beat frequency, and the physical parameter such as temperature and strain can be defined from the wavelength of the VCSEL. In addition to monitoring temperature and strain, the developed system can be improved to identify various physical parameters such as stress, crack, and load in the monitored structure.

For practical application of the proposed system to the SHMS, we have to increase the number of FBGs. Although we have demonstrated three FBGs in the range of 6.6 km, it would be possible to involve many FBGs in large-scale SHMS. In our experiments, we used FBGs with about 5% reflectiviy, and then only 20 FBGs can be installed. Although large number of FGBs is effective for precise SHMS, the cost of the SHMS is increased. In reference [16], 17 FBGs are used for the SHMS of a 500 m-long bridge. More then 100 FBGs will be used for the SHMS of over 1 km-long bridge. One of the method to increase the number of FBGs up to 100 is using FBGs with low reflectivity for example 1%. The other method to increase the number of FBGs is spatial multiplexing of FBG sensor arrays. The laser light from a VCSEL is switched between the FBG sensor arrays by using a multi-channel optical switch. For example, if the number of FBGs for each FBG sensor array is 50 and five FBG sensor arrays are spatial multiplexed using multi-channel optical switch, totally 250 FBGs can be installed for the SHMS. However, it needs further study on the effect of the number of FBGs in long-range by using the I-FMCW optical ranging system.

We have demonstrated the stability of the proposed system for 23 hours as temperature sensor in laboratory. However, more long-time (for months and years) field study of the proposed system is needed to validate effectiveness of detecting physical parameter change caused by damage of structures.

## References


[1] P. Ferdinand, “The Evolution of Optical Fiber Sensors Technologies During the 35 Last Years and Their Applications in Structure Health Monitoring,” in *7th EWSHM*, 2014.

[2] M. Ramakhrisnan, G. Rajan, Y. Semenova, and G. Farrell, “Overview of Fiber Optic Sensor Technologies for Strain / Temperature Sensing Applications in Composite Material,” *Sensors*, vol. 16, no. 99, pp. 1–27, 2016.

[3] R. Rajinikumar, M. Suesser, K. G. Narayankhedkar, G. Krieg, and M. D. Atrey, “Fiber Bragg Grating Sensors for Measuring Temperature and Strain Simultaneously at Cryogenic Temperature,” in *AIP Conference Proceedings*, 2008, vol. 985, pp. 383–390.

[4] V. R. Pachava, S. Kamineni, S. S. Madhuvarasu, K. Putha, and V. R. Mamidi, “FBG Based High Sensitive Pressure Sensor and Its Low-Cost Interrogation System With Enhanced Resolution,” *Photonic Sensors*, vol. 5, no. 4, pp. 321–329, 2015.

[5] B. Das and V. Chandra, “Fiber-MZI-based FBG sensor interrogation : comparative study with a CCD spectrometer,” *Appl. Opt.*, vol. 55, no. 29, pp. 8287–8292, 2016.

[6] J. Chen, B. Liu, and H. Zhang, “Review of fiber Bragg grating sensor technology,” *Front. Eptoelectron. China*, vol. 4, no. 2, pp. 204–212, 2011.

[7] S. Yamashita, Y. Nakazaki, R. Konishi, and O. Kusakari, “Wide and Fast Wavelength-Swept Fiber Laser Based on Dispersion Tuning for Dynamic Sensing,” *J. sensors*, vol. 2009, pp. 1–12, 2009.

[8] S. Moon and E. S. Choi, “VCSEL-based swept source for low-cost optical coherence tomography,” *Biomed. Opt. Express*, vol. 8, no. 2, pp. 19712–19723, 2017.

[9] C. S. Shin and C. Chiang, “Deformation monitoring by using optical fiber grating sensor,” *J. Chinese Inst. Eng.*, vol. 28, no. 6, pp. 985–992, 2005.

[10] W. Stewart, B. Van Hoe, G. Van Steenberge, S. Schultz, and K. Peters, “Spectral profile tracking of multiplexed fi ber Bragg grating sensors,” *Opt. Commun.*, vol. 357, pp. 113–119, 2015.

[11] A. Barrias, J. R. Casas, and S. Villalba, “A Review of Distributed Optical Fiber Sensors for Civil Engineering Applications,” *Sensors*, vol. 16, no. 748, pp. 1–35, 2016.

[12] Y. Tanaka and H. Miyasawa, “Multipoint Fiber Bragg Grating Sensing Using Two-Photon Absorption Process in Silicon Avalanche Photodiode,” *J. Light. Technol.*, vol. 36, no. 4, pp. 1032–1038, 2018.

[13] T. Hariyama, P. A. . Sandborn, M. Watanabe, and M. C. Wu, “High-accuracy range-sensing system based on FMCW using low-cost VCSEL,” *Opt. Express*, vol. 26, no. 7, pp. 1496–1503, 2018.

[14] K. Yuksel, M. Wuilpart, V. Moeyaert, and P. Mégret, “Optical Frequency Domain Reflectometry : A Review,” in *ICTON*, 2009, pp. 3–7.

[15] S. Werzinger, S. Bergdolt, R. Engelbrecht, T. Thiel, and B. Schmauss, “Quasi-Distributed Fiber Bragg Grating Sensing Using Stepped Incoherent Optical Frequency Domain Reflectometry,” *J. Light. Technol.*, vol. 34, no. 22, pp. 5270–5277, 2016.

[16] M. Nishio, “Quality Evaluation of Fiber-Optic Strain Data Acquired in Long-Term Bridge Monitoring,” *Sensors Mater.*, vol. 29, no. 2, pp. 141–152, 2017.

[17] K. Iiyama, S. Matsui, T. Kobayashi, and T. Maruyama, “High-Resolution FMCW Reflectometry Using a Single-Mode Vertical-Cavity Surface-Emitting Laser,” *IEEE Photonics Technol. Lett.*, vol. 23, no. 11, pp. 703–705, 2011.

[18] D. Tosi, “Review and Analysis of Peak Tracking techniques for Fiber Bragg Grating Sensors,” *Sensors*, vol. 17, no. 2368, pp. 1–35, 2017.

[19] H. T. Wang, B. Zhao, Y. Dai, and G. Huang, “Fiber Bragg Grating Sensor for Strain Sensing in Low Temperature Superconducting Magnet,” *IEEE Trans. Appl. Supercond.*, vol. 20, no. 3, pp. 1798–1801, 2010.

[20] M. Enckell, B. Glisic, F. Myrvoll, and B. Bergstrand, “Evaluation of a large-scale bridge strain , temperature and crack monitoring with distributed fibre optic sensors,” *J. Civ. Struct Heal. Monit*, vol. 1, pp. 37–46, 2011.

[21] R. K. Ula, Y. Noguchi, and K. Iiyama, “Three-Dimensional Object Profiling Using Highly Accurate FMCW Optical Ranging System,” *J. Light. Technol.*, vol. 37, no. 15, pp. 3826–3833, 2019.

[22] L. Chen, X. Bao, J. Song, W. Li, P. Lu, and Y. Xu, “Long-Range High Spatial Resolution Distributed Temperature and Strain Sensing Based on Optical Frequency-Domain Reflectometry,” *IEEE Photonics J.*, vol. 6, no. 3, pp. 1–8, 2014.

[23] M. Maheshwari, S. Chuan, Y. Yang, and A. Asundi, “Wavelength-shifted chirped FBGs for temperature compensated strain measurement,” *Sensors Actuators A. Phys.*, vol. 265, pp. 231–235, 2017.

[24] P. Lu, L. Men, and Q. Chen, “Resolving cross sensitivity of fiber Bragg gratings with different polymeric coatings,” *Appl. Phys. Lett.*, vol. 92, no. 171112, pp. 1–3, 2008.

**Dwi Hanto** was born in Sukoharjo, Indonesia, in 1984. He received a Bachelor's degree in Physics from University of Sebelas Maret in 2008, and a Master's degree in Instrumental Physics from University of Indonesia in 2012. From 2009, he has been working at the Optoelectronics Laboratory, Research Center for Physics, Indonesian Institute of Sciences (LIPI). He is currently working towards the Ph.D. degree at the Division of Electrical and Computer Science, Kanazawa University. His principle research interests include fiber optic sensors, optoelectronics, and instrumental physics. He is a member of the Optical Society of America (OSA), Indonesian Researcher Union, Physical Society of Indonesia (PSI), and IEEE.

**Koichi Iiyama** was born in Fukui, Japan in 1963. He received the B.E, M.E, and D.E degrees in Electronics from Kanazawa University in 1985, 1987, and 1993, respectively. From 1987 to 1988, he was with Yokogawa Hewlett-Packard, Ltd. Since 1988, he has been with Kanazawa University, where he is currently a Professor. From 2001 to 2002, he was a guest scientist with Heinrich-Hertz-Institut für Nachrichtentechnik Berlin GmbH, Berlin, Germany. He is now working in research on optical ranging system, optical imaging, and optical fiber science. He is a member of the IEICE, the Japan Society of Applied Physics, and IEEE.